Thermal Relaxation and Coherence Dynamics of Spin 3/2. I. Static and Fluctuating Quadrupolar Interactions in the Multipole Basis

JOHAN R.C. VAN DER MAAREL

Leiden Institute of Chemistry, Leiden University, Leiden, The Netherlands

ABSTRACT: The relaxation dynamics of the spin 3/2 density operator in the presence of fluctuating and static quadrupolar interactions is reviewed. The nuclear magnetic resonance (NMR) line shapes are analyzed for any value of the static quadrupolar interaction, ranging from isotropic systems to systems exhibiting large splitting far exceeding the line widths. Pulse sequences optimized for the elimination of line broadening due to an inhomogeneous static quadrupolar interaction and for the detection of nuclei involved in slow molecular motion and/or in anisotropic, liquid crystalline environment are discussed. In Part II, the dynamics of spin 3/2 in the presence of a (pulsed) radio frequency (RF) field is reviewed. Concepts Magn Reson Part A 19A: 97–116, 2003

KEY WORDS: nuclear magnetic relaxation; quadrupolar nuclei; multiple-quantum spectroscopy; liquid crystal

INTRODUCTION

Quadrupolar spin probes are becoming increasingly important in a wide range of applications ranging from the investigation of porous materials (*1*), (bio)polymers in the liquid state (*2–6*), through biological fluids (*7*), to the diagnosis of pathology in humans via magnetic resonance imaging (MRI) (*8*). Among those probes, the naturally occurring spin quantum number 3/2 nuclei ^{7}Li, ^{23}Na, ^{39}K, ^{87}Rb, ^{35}Cl, ^{81}Br, and ^{131}Xe constitute an important class. The quadrupolar interaction, which is essentially a tensor property, is determined by the orientation, magnitude, and temporal duration of electric field gradients (EFGs) generated by the surrounding medium (*9*) and/or the electronic configuration around the nu-

Received 8 April 2003; revised 2 July 2003; accepted 2 July 2003

Correspondence to: Johan R.C. van der Maarel; E-mail: j.maarel@chem.leidenuniv.nl

Concepts in Magnetic Resonance Part A, Vol. 19A(2) 97–116 (2003)

Published online in Wiley InterScience (www.interscience.wiley.com). DOI 10.1002/cmr.a.10087

Table 1 Irreducible Tensor Operators for Spin $I = 3/2$ (*11*)*

$T_{00} = 1$	$T_{20} = 1/\sqrt{6}(3I_z^2 - I(I+1))$	$T_{30} = 1/\sqrt{10}(5I_z^3 - (3I(I+1) - 1)I_z)$
$T_{10} = I_z$	$T_{2\pm1} = \mp 1/2[I_z, I_\pm]_+$	$T_{3\pm1} = \mp 1/4\sqrt{3/10}[5I_z^3 - I(I+1) - 1/2, I_\pm]_+$
$T_{1\pm1} = \mp 1/\sqrt{2}I_\pm$	$T_{2\pm2} = 1/2I_\pm^2$	$T_{3\pm2} = 1/2\sqrt{3/4}[I_z, I_\pm^2]_+$
		$T_{3\pm3} = \mp 1/2\sqrt{1/2}I_\pm^3$

* The unit tensors are related to their nonunit counterparts according to $\hat{T}_{00} = 1/2T_{00}$, $\hat{T}_{1m} = 1/\sqrt{5}T_{1m}$, $\hat{T}_{2m} = 1/2\sqrt{2/3}T_{2m}$, and $\hat{T}_{3m} = 1/3\sqrt{2}T_{3m}$.

cleus. If the motions are rapid and all orientations are equally probable (isotropic system), the quadrupolar interaction is averaged to zero on the timescale of the inverse Larmor frequency. However, in anisotropically oriented systems such as liquid crystals, the nuclei may experience a nonvanishing average EFG. This static coupling induces a shift in the energy levels of the spin system and, consequently, the spectrum shows a frequency splitting. This splitting can be taken as indication of the extent to which the system is macroscopically ordered.

For spin 3/2 in the Redfield regime, where relaxation is described by second-order perturbation theory, the spin dynamics can be solved in closed analytical form. Longitudinal relaxation gives information about relatively fast motions, whereas slow dynamics is probed by transverse relaxation or by applying a lock through a radio-frequency (RF) field (*10*). Here, I will review the classical relaxation and evolution in the Larmor frequency–rotating frame; relaxation in the presence of a (pulsed) RF field is reviewed in part II. To describe the spin dynamics, extensive use will be made of the irreducible tensor operator representation. The advantage of this representation is that it is relatively easy to follow the rank and coherence order of the density operator in a complicated sequence of RF pulses and evolution periods. The formalism describing the time evolution of the spin 3/2 system under the action of RF pulses and static and fluctuating quadrupolar interactions will be reviewed. With the help of this formalism, it is relatively easy to understand and design complicated pulse sequences serving various purposes. Apart from the measurement of the dynamic properties (the spectral density of the fluctuating quadrupolar interaction), these purposes include the selective detection of nuclei (ions) involved in slow molecular motion and/or those experiencing a (possibly hidden) static quadrupolar coupling. Finally, I will also discuss acquisition schemes optimized for the elimination of line broadening due to an inhomogeneous static quadrupolar interaction through the sample.

TENSOR OPERATOR FORMALISM

Basis Operators

Throughout this review, we express the density operator and Hamiltonians in terms of irreducible tensor operators (see Table 1). Commutation relationships are conveniently tabulated by Bowden et al. (*11, 12*). Orthonormal unit tensor operators $\hat{T}_{lm}$, indicated by a cap hat, also are introduced. The latter operators satisfy the orthonormality relationship $\mathrm{Tr}\{\hat{T}_{lm}\hat{T}^\dagger_{l'm'}\} = \delta_{ll'}\delta_{mm'}$ with $\hat{T}^\dagger_{lm} = (-1)^m\hat{T}_{l-m}$. For spin quantum number $I = 3/2$, the unit tensors are related to their T_{lm} counterparts according to $\hat{T}_{00} = 1/2T_{00}$, $\hat{T}_{1m} = 1/\sqrt{5}T_{1m}$, $\hat{T}_{2m} = 1/2\sqrt{2/3}T_{2m}$, and $\hat{T}_{3m} = 1/3\sqrt{2}T_{3m}$. To reflect the Hermitian nature, it also is convenient to define symmetric and antisymmetric combinations:

$$T_{lm}(s) = 1/\sqrt{2}\,(T_{l-m} + T_{lm})$$
$$T_{lm}(a) = 1/\sqrt{2}\,(T_{l-m} - T_{lm}) \qquad [1]$$

For the unit tensor operators, these combinations are defined analogously. The density operator is expanded in 16 basis operators: $\hat{T}_{00}$ (the identity), $\hat{T}_{10} = 1/\sqrt{5}I_z$ (proportional to longitudinal magnetization), $\hat{T}_{11}(a) = 1/\sqrt{5}I_x$ and $\hat{T}_{11}(s) = -i/\sqrt{5}I_y$ (proportional to the x- and y-magnetization, respectively), $\hat{T}_{20}$ (quadrupolar spin polarization), $\hat{T}_{21}(s)$ and $\hat{T}_{21}(a)$ (rank-two single-quantum coherences), $\hat{T}_{22}(s)$ and $\hat{T}_{22}(a)$ (rank-two double-quantum coherences), $\hat{T}_{30}$ (octopolar spin polarization), $\hat{T}_{31}(s)$ and $\hat{T}_{31}(a)$ (rank-three single-quantum coherences), $\hat{T}_{32}(s)$ and $\hat{T}_{32}(a)$ (rank-three double-quantum coherences), and $\hat{T}_{33}(s)$ and $\hat{T}_{33}(a)$ (rank-three triple-quantum coherences).

A major advantage of the tensor operators is that we can exploit fully their rotational properties for the effects of RF pulses and evolution under the action of static and fluctuating quadrupolar interactions. Furthermore, the 15 relevant operators form an irreducible basis set, in contrast with the popular fictitious spin-$\frac{1}{2}$ operators. As shown by Bowden et al., the latter set is redundant (there are 18 fictitious spin-$\frac{1}{2}$ operators)

and almost every operator is composed of irreducible tensor operators differing in rank (*12*). Accordingly, using fictitious spin-$\frac{1}{2}$ operators, it is difficult to follow the rank of the tensors in a complicated sequence of RF pulses and evolution intervals. In this respect, the design and understanding of pulse sequences is more transparent if irreducible tensor operators are used.

Hamiltonians

The spin system evolves under the (possibly simultaneous) action of the Zeeman, RF, static quadrupolar, and fluctuating quadrupolar Hamiltonians. The calculations reported in this review refer to an interaction representation in which the Zeeman Hamiltonian $H_Z = \omega_0 T_{10}$ vanishes. The density operator and Hamiltonians in this Larmor frequency–rotating frame are indicated by the asterisk. With the RF field applied exactly on resonance along the x-axis with field strength $\omega_1 = -\gamma B_1$, the corresponding Hamiltonian is time independent and reads

$$H_1^* = \omega_1 I_x = \omega_1 T_{11}(a) = \sqrt{5}\omega_1 \hat{T}_{11}(a) \qquad [2]$$

Throughout this review, the sign conventions and angle definitions of Rose are adopted (*13*).

For simplicity, we will only consider a static quadrupolar interaction with cylindrical symmetry. The static quadrupolar Hamiltonian commutes with the Zeeman Hamiltonian and takes the form

$$H_{QS}^* = \omega_Q[3I_z^2 - I(I+1)]/6 = \omega_Q \hat{T}_{20} \qquad [3]$$

where ω_Q denotes the residual quadrupolar interaction parameter. The latter coupling parameter represents the part of the quadrupolar interaction that persists after motional averaging and is not to be confused with the root-mean-square average of the fluctuating part. The static quadrupolar interaction is either uniform or inhomogeneous across the sample. In the former situation, clear quadrupolar splitting in the spectra is observed (provided the splitting exceeds the line widths). In the case of a nonuniformly aligned system, the sample often is assumed composed of domains, each domain characterized by a local director and all of the domains having the same dynamic properties. Furthermore, the exchange among the domains usually is slow on a timescale exceeding the inverse line widths and/or splitting, so that the observed spectrum represents a static average over all domains. Each domain is characterized by a residual quadrupolar coupling

$$\omega_Q = \bar{\omega}_Q(3\cos^2\theta - 1)/2 \qquad [4]$$

with θ the angle between the local director and the direction of the main magnetic field B_0 and $\bar{\omega}_Q$ denotes the maximum splitting measured for $\theta = 0$. In first order, the frequency of the central transition is unaffected, but, depending on the distribution in values of θ, the satellites are now spread out over a large frequency range (*10*). In particular, the broadening of the satellites caused by this inhomogeneity in static quadrupolar coupling calls for sophisticated pulse sequences in order to extract reliable information concerning molecular dynamics.

The zero-average *fluctuating* part of the quadrupolar interaction can be expressed as

$$H_{QF}^*(t) = C_Q \sum_{m=-2}^{2} (-1)^m T_{2m} \times \exp(im\omega_0 t)[F_{2-m}(t) - \langle F_{2-m}\rangle] \qquad [5]$$

Here $C_Q = eQ/(\hbar\sqrt{6})$, where Q is the quadrupolar moment of the nucleus and the other symbols have their usual meaning. The EFG tensor components F_{2m} take the form $F_{20} = 1/2V_{zz}$, $F_{2\pm1} = \mp 1/\sqrt{6}(V_{xz} \pm iV_{yz})$, and $F_{2\pm2} = 1/(2\sqrt{6})\ (V_{xx} - V_{yy} \pm 2iV_{xy})$ and $\langle F_{2m}\rangle$ represents their average values. The EFG components are time dependent because of molecular motion. The fluctuating EFG can be generated by, e.g., atomic charges on colloidal particles and/or macromolecules, small ions, and contributions from the ion hydration shell. I will not discuss further the source of the fluctuating quadrupolar interactions or the various mechanisms causing the loss of correlation, but a good review is available (*14*). Here, we will focus on the spin dynamics by a full analysis of the time evolution of the density operator.

TIME EVOLUTION OF THE DENSITY OPERATOR

The master equation of the time evolution of the density operator under a static Hamiltonian H_S^* is given by (*10*)

$$d\sigma^*/dt = -i[H_S^*, \sigma^*] \qquad [6]$$

where the static Hamiltonian may include the RF and the static quadrupolar Hamiltonians $H_S^* = H_1^* + H_{QS}^*$. The effect of the fluctuating quadrupolar interaction Hamiltonian $H_{QF}^*(t)$ can be considered in the framework of the Redfield relaxation theory. The conditions for the validity of this second-order perturbation theory are that

changes in the density operator are small on the timescale τ_c of the lattice motions $\langle H^{*2}_{QF}\rangle\tau_c^2 \ll 1$. This often is the case in soft-condensed matter, where the correlation times can be rather long, but with relatively small values of the corresponding coupling constants. Equation [6] now becomes

$$d\sigma^*/dt = -i[H^*_S, \sigma^*] + f(\sigma^*) \qquad [7]$$

with the relaxation superoperator

$$f(\sigma^*) = -\int_0^\infty \langle [H^*_{QF}(t), [\exp(-iH^*_S\tau)H^*_{QF}(t-\tau)\exp(iH^*_S\tau), \sigma^*(t)]]\rangle d\tau \qquad [8]$$

In the presence of static and fluctuating quadrupolar interactions only (i.e., in the absence of an RF field), the static Hamiltonian $H^*_S = H^*_{QS}$ commutes with $H^*_{QF}(t)$ and, accordingly, is seen to vanish in the relaxation superoperator. Furthermore, if the EFG is completely averaged to zero by molecular motion, $H^*_S = 0$ and the time dependence is given by the relaxation contribution only. Here, we will deal exclusively with relaxation dynamics in the absence of an RF field; relaxation in the presence of an RF field is reviewed in part II.

EFFECT OF RF PULSES

As an illustration how the spin operators transform under rotations, first, we will analyze the effect of RF pulses. The resulting rotation properties are particularly useful in the analysis and description of coherence transfer experiments. First, we will assume that the static and fluctuating quadrupolar interactions can be neglected during the pulse. It should be noticed that this approximation is particularly poor in the case of long, soft pulses and/or in the presence of large quadrupolar splitting.

Hard Pulses

The RF field is applied exactly on resonance along the x-axis during a period τ and is described by the Hamiltonian in Eq. [2]. The time evolution of the density operator is given by Eq. [6] with $H^*_S = H^*_1$

$$d\sigma^*/dt = -i[H^*_1, \sigma^*] = -i\omega_1[T_{11}(a), \sigma^*] \qquad [9]$$

and has the formal solution $\sigma^*(t) = \exp(-iH^*_1t)\sigma^*(0)\exp(iH^*_1t)$. With the commutation relations (*12*), this equation reduces to five sets of coupled differential equations

$$\frac{d}{dt}\begin{pmatrix}\hat{T}_{10}\\ \hat{T}_{11}(s)\end{pmatrix} = \begin{pmatrix}0 & -i\omega_1\\ -i\omega_1 & 0\end{pmatrix}\begin{pmatrix}\hat{T}_{10}\\ \hat{T}_{11}(s)\end{pmatrix}$$

$$\frac{d}{dt}\begin{pmatrix}\hat{T}_{21}(a)\\ \hat{T}_{22}(a)\end{pmatrix} = \begin{pmatrix}0 & -i\omega_1\\ -i\omega_1 & 0\end{pmatrix}\begin{pmatrix}\hat{T}_{21}(a)\\ \hat{T}_{22}(a)\end{pmatrix}$$

$$\frac{d}{dt}\begin{pmatrix}\hat{T}_{20}\\ \hat{T}_{21}(s)\\ \hat{T}_{22}(s)\end{pmatrix} = \begin{pmatrix}0 & -i\sqrt{3}\omega_1 & 0\\ -i\sqrt{3}\omega_1 & 0 & -i\omega_1\\ 0 & -i\omega_1 & 0\end{pmatrix}\begin{pmatrix}\hat{T}_{20}\\ \hat{T}_{21}(s)\\ \hat{T}_{22}(s)\end{pmatrix}$$

$$\frac{d}{dt}\begin{pmatrix}\hat{T}_{31}(a)\\ \hat{T}_{32}(a)\\ \hat{T}_{33}(a)\end{pmatrix} = \begin{pmatrix}0 & -i\sqrt{5/2}\omega_1 & 0\\ -i\sqrt{5/2}\omega_1 & 0 & -i\sqrt{3/2}\omega_1\\ 0 & -i\sqrt{3/2}\omega_1 & 0\end{pmatrix}\begin{pmatrix}\hat{T}_{31}(a)\\ \hat{T}_{32}(a)\\ \hat{T}_{33}(a)\end{pmatrix}$$

$$\frac{d}{dt}\begin{pmatrix}\hat{T}_{30}\\ \hat{T}_{31}(s)\\ \hat{T}_{32}(s)\\ \hat{T}_{33}(s)\end{pmatrix} = \begin{pmatrix}0 & -i\sqrt{6}\omega_1 & 0 & 0\\ -i\sqrt{6}\omega_1 & 0 & -i\sqrt{5/2}\omega_1 & 0\\ 0 & -i\sqrt{5/2}\omega_1 & 0 & -i\sqrt{3/2}\omega_1\\ 0 & 0 & -i\sqrt{3/2}\omega_1 & 0\end{pmatrix}\begin{pmatrix}\hat{T}_{30}\\ \hat{T}_{31}(s)\\ \hat{T}_{32}(s)\\ \hat{T}_{33}(s)\end{pmatrix} \qquad [10]$$

Table 2 The Evolution of the Tensor Operators Under the Influence of a Hard RF Pulse with Pulse Angle $\beta = \omega_1\tau = -\gamma B_1\tau$ Along the *x*-Axis in the Rotating Frame

U	$\exp(-i\beta I_x)U\ \exp(i\beta I_x)$
$\hat{T}_{10}$	$\hat{T}_{10}\cos(\beta) - i\hat{T}_{11}(s)\sin(\beta)$
$\hat{T}_{11}(a)$	$\hat{T}_{11}(a)$
$\hat{T}_{11}(s)$	$-i\hat{T}_{10}\sin(\beta) + \hat{T}_{11}(s)\cos(\beta)$
$\hat{T}_{20}$	$\hat{T}_{20}1/4(3\cos(2\beta) + 1) - i\hat{T}_{21}(s)1/2\sqrt{3}\sin(2\beta) - \hat{T}_{22}(s)1/2\sqrt{3}\sin^2(\beta)$
$\hat{T}_{21}(a)$	$\hat{T}_{21}(a)\cos(\beta) - i\hat{T}_{22}(a)\sin(\beta)$
$\hat{T}_{21}(s)$	$-i\hat{T}_{20}1/2\sqrt{3}\sin(2\beta) + \hat{T}_{21}(s)\cos(2\beta) - i\hat{T}_{22}(s)1/2\sin(2\beta)$
$\hat{T}_{22}(a)$	$-i\hat{T}_{21}(a)\sin(\beta) + \hat{T}_{22}(a)\cos(\beta)$
$\hat{T}_{22}(s)$	$-\hat{T}_{20}1/2\sqrt{3}\sin^2(\beta) - i\hat{T}_{21}(s)1/2\sin(2\beta) + \hat{T}_{22}(s)1/4(\cos(2\beta) + 3)$
$\hat{T}_{30}$	$\hat{T}_{30}1/8(3\cos(\beta) + 5\cos(3\beta)) - i\hat{T}_{31}(s)1/8\sqrt{3/2}(\sin(\beta) + 5\sin(3\beta)) - \hat{T}_{32}(s)1/2\sqrt{15}\cos(\beta)\sin^2(\beta) + i\hat{T}_{33}(s)1/2\sqrt{5/2}\sin^3(\beta)$
$\hat{T}_{31}(a)$	$\hat{T}_{31}(a)1/8(5\cos(2\beta) + 3) - i\hat{T}_{32}(a)1/2\sqrt{5/2}\sin(2\beta) - \hat{T}_{33}(a)1/4\sqrt{15}\sin^2(\beta)$
$\hat{T}_{31}(s)$	$-i\hat{T}_{30}1/8\sqrt{3/2}(\sin(\beta) + 5\sin(3\beta)) + \hat{T}_{31}(s)1/16(\cos(\beta) + 15\cos(3\beta)) + i\hat{T}_{32}(s)1/8\sqrt{5/2}(\sin(\beta) - 3\sin(3\beta)) - \hat{T}_{33}(s)1/4\sqrt{15}\cos(\beta)\sin^2(\beta)$
$\hat{T}_{32}(a)$	$-i\hat{T}_{31}(a)1/2\sqrt{5/2}\sin(2\beta) + \hat{T}_{32}(a)\cos(2\beta) - i\hat{T}_{33}(a)1/2\sqrt{3/2}\sin(2\beta)$
$\hat{T}_{32}(s)$	$-\hat{T}_{30}1/2\sqrt{15}\cos(\beta)\sin^2(\beta) + i\hat{T}_{31}(s)1/8\sqrt{5/2}(\sin(\beta) - 3\sin(3\beta)) + \hat{T}_{32}(s)1/8(5\cos(\beta) + 3\cos(3\beta)) - i\hat{T}_{33}(s)1/8\sqrt{3/2}(5\sin(\beta) + \sin(3\beta))$
$\hat{T}_{33}(a)$	$-\hat{T}_{31}(a)1/4\sqrt{15}\sin^2(\beta) - i\hat{T}_{32}(a)1/2\sqrt{3/2}\sin(2\beta) + \hat{T}_{33}(a)1/8(3\cos(2\beta) + 5)$
$\hat{T}_{33}(s)$	$i\hat{T}_{30}1/2\sqrt{5/2}\sin^3(\beta) - \hat{T}_{31}(s)1/4\sqrt{15}\cos(\beta)\sin^2(\beta) - i\hat{T}_{32}(s)1/8\sqrt{3/2}(5\sin(\beta) + \sin(3\beta)) + \hat{T}_{33}(s)1/8\cos(\beta)(\cos(2\beta) + 7)$

In these sets of differential equations, it is seen that tensors differing in rank are decoupled. Under a hard RF pulse, the rank of the tensor operators is conserved, whereas the order might change. As we will see shortly, this is complementary to the effect of relaxation, where the order is conserved and the rank might change.

The differential equations can be diagonalized and subsequently integrated in analytical form. The general form of the differential equations is $d\mathbf{T}/dt = \mathbf{MT}$ where $\mathbf{T}$ represents a vector with the tensor operators as elements and $\mathbf{M}$ is a symmetric matrix. If we denote $\mathbf{M}_D$ the diagonal form of the matrix $\mathbf{M}$ and by S the similarity transform obtained from the eigenvectors of $\mathbf{M}$, then $\mathbf{M}_D = S^{-1}\mathbf{M}S$ and the solution reads $\mathbf{T}(\tau) = S\exp(\mathbf{M}_D\tau)S^{-1}\mathbf{T}(0)$ with $\mathbf{T}(0)$ the initial condition. The analytical calculations are most conveniently done with a computing environment like *Mathematica* (Wolfram Research, Champaign, IL). For each operator, the solution is set out in Table 2 with the pulse angle $\beta = \omega_1\tau = -\gamma B_1\tau$. These results represent a tensor rotation about the *x*-axis, which is related to symmetric and antisymmetric combinations of the Wigner rotation matrix elements. It should be noticed that, because of the sign conventions, for a rotation over a *positive* angle β, the B_1 field should be applied along the *negative* *x*-axis.

If a phase ϕ is associated with the hard pulse, the reference coordinate system is first rotated over an angle ϕ about the *z*-axis such that the pulse is along the *x*-axis of the new frame of reference. This rotation of the base results in a transformation of the tensor operators according to

$$\hat{T}_{lm}(s) \rightarrow \hat{T}_{lm}(s)\cos(m\phi) + i\hat{T}_{lm}(a)\sin(m\phi)$$
$$\hat{T}_{lm}(a) \rightarrow \hat{T}_{lm}(a)\cos(m\phi) + i\hat{T}_{lm}(s)\sin(m\phi) \quad [11]$$

In the new frame of reference, the effect of the pulse can be evaluated with the results in Table 2. Finally, the frame is returned to its original state by a reverse rotation over angle $-\phi$. For ease of reference, the effect of a hard ($\beta = -\gamma B_1\tau = \pi/2$) pulse along the *x*- and the *y*-axis are collected in Table 3.

Soft Pulses

If the static quadrupolar Hamiltonian can not be neglected during the pulse, the time evolution of the density operator takes the form

$$d\sigma^*/dt = -i[\omega_1 T_{11}(a) + 1/\sqrt{6}\omega_Q T_{20}, \sigma^*] \quad [12]$$

which now reduces to two sets of coupled differential equations. The first one is

$$\frac{d}{dt}\begin{pmatrix}\hat{T}_{11}(a)\\ \hat{T}_{20}\\ \hat{T}_{21}(s)\\ \hat{T}_{22}(s)\\ \hat{T}_{31}(a)\\ \hat{T}_{32}(a)\\ \hat{T}_{33}(a)\end{pmatrix}=\begin{pmatrix}0 & 0 & i\sqrt{3/5}\omega_Q & 0 & 0 & 0 & 0\\ 0 & 0 & -i\sqrt{3}\omega_1 & 0 & 0 & 0 & 0\\ i\sqrt{3/5}\omega_Q & -i\sqrt{3}\omega_1 & 0 & -i\omega_1 & i\sqrt{2/5}\omega_Q & 0 & 0\\ 0 & 0 & -i\omega_1 & 0 & 0 & i\omega_Q & 0\\ 0 & 0 & i\sqrt{2/5}\omega_Q & 0 & 0 & -i\sqrt{5/2}\omega_1 & 0\\ 0 & 0 & 0 & i\omega_Q & -i\sqrt{5/2}\omega_1 & 0 & -i\sqrt{3/2}\omega_1\\ 0 & 0 & 0 & 0 & 0 & -i\sqrt{3/2}\omega_1 & 0\end{pmatrix}\begin{pmatrix}\hat{T}_{11}(a)\\ \hat{T}_{20}\\ \hat{T}_{21}(s)\\ \hat{T}_{22}(s)\\ \hat{T}_{31}(a)\\ \hat{T}_{32}(a)\\ \hat{T}_{33}(a)\end{pmatrix} \quad [13]$$

and for the second set one has

$$\frac{d}{dt}\begin{pmatrix}\hat{T}_{10}\\ \hat{T}_{11}(s)\\ \hat{T}_{21}(a)\\ \hat{T}_{22}(a)\\ \hat{T}_{30}\\ \hat{T}_{31}(s)\\ \hat{T}_{32}(s)\\ \hat{T}_{33}(s)\end{pmatrix}=\begin{pmatrix}0 & -i\omega_1 & 0 & 0 & 0 & 0 & 0 & 0\\ -i\omega_1 & 0 & i\sqrt{3/5}\omega_Q & 0 & 0 & 0 & 0 & 0\\ 0 & i\sqrt{3/5}\omega_Q & 0 & -i\omega_1 & 0 & i\sqrt{2/5}\omega_Q & 0 & 0\\ 0 & 0 & -i\omega_1 & 0 & 0 & 0 & i\omega_Q & 0\\ 0 & 0 & 0 & 0 & 0 & -i\sqrt{6}\omega_1 & 0 & 0\\ 0 & 0 & i\sqrt{2/5}\omega_Q & 0 & -i\sqrt{6}\omega_1 & 0 & -i\sqrt{5/2}\omega_1 & 0\\ 0 & 0 & 0 & i\omega_Q & 0 & -i\sqrt{5/2}\omega_1 & 0 & -i\sqrt{3/2}\omega_1\\ 0 & 0 & 0 & 0 & 0 & 0 & -i\sqrt{3/2}\omega_1 & 0\end{pmatrix}\begin{pmatrix}\hat{T}_{10}\\ \hat{T}_{11}(s)\\ \hat{T}_{21}(a)\\ \hat{T}_{22}(a)\\ \hat{T}_{30}\\ \hat{T}_{31}(s)\\ \hat{T}_{32}(s)\\ \hat{T}_{33}(s)\end{pmatrix} \quad [14]$$

Although the matrices in Eqs. [13] and [14] can be solved easily by numerical methods, they can be diagonalized and the differential equations can be integrated in analytical form (*15, 16*). Equation [13] contains the tensor operator $\hat{T}_{11}(a)$ along the RF field and is particularly relevant for the description of the spin-lock experiment (*17, 18*). The matrix in Eq. [13] has a three-dimensional (3D) null space and four nonzero, imaginary eigenvalues $\pm i\lambda_{1,2}$, being

$$\lambda_1 = \sqrt{\omega_Q^2 + 2\omega_1\omega_Q + 4\omega_1^2},$$
$$\lambda_2 = \sqrt{\omega_Q^2 - 2\omega_1\omega_Q + 4\omega_1^2} \quad [15]$$

whereas the matrix in Eq. [14] has eight imaginary eigenvalues $\pm i\lambda_{3,4,5,6}$

$$\lambda_3 = \omega_1 + 1/\sqrt{2}\ \sqrt{\omega_Q^2 + 4\omega_1^2 + \lambda_1\lambda_2},$$
$$\lambda_4 = \omega_1 + 1/\sqrt{2}\ \sqrt{\omega_Q^2 + 4\omega_1^2 - \lambda_1\lambda_2}$$
$$\lambda_5 = \omega_1 - 1/\sqrt{2}\ \sqrt{\omega_Q^2 + 4\omega_1^2 + \lambda_1\lambda_2},$$
$$\lambda_6 = \omega_1 - 1/\sqrt{2}\ \sqrt{\omega_Q^2 + 4\omega_1^2 - \lambda_1\lambda_2} \quad [16]$$

The resulting time dependencies of the basis operators are rather complicated functions and have been set out by Campolieti et al. (*19*). In the case of *soft* pulses and in the presence of a static quadrupolar interaction of comparable strength, both the order and rank of the tensor operators can change. In Part II, the signal loss due to relaxation during the RF pulses will be reviewed.

THERMAL RELAXATION IN ISOTROPIC ENVIRONMENT

The effects of thermal relaxation are important in determining both the shape and the widths of the spin 3/2 resonance. First, we will consider the simplest situation, i.e., relaxation in a medium where the EFG is averaged completely to zero by molecular dynamics on a timescale faster than the inverse line widths. These media are classified operationally as being *isotropic,* which essentially means that there is no long-range position and/or orientation order. In an isotropic environment, the EFG is averaged completely to zero by molecular motion $\langle F_{2m}\rangle = 0$. Furthermore, here we consider relaxation in the absence of RF irradiation so that $H_S^* = 0$. Accordingly, the only relevant Hamiltonian is the fluctuating quadrupolar interaction $H_{QF}^*(t)$ and the master equation takes the form

Table 3 The Evolution of the Tensor Operators Under the Influence of a Hard RF Pulse with Pulse Angle $\beta = -\gamma B_1 \tau = \pi/2$ Along the *x*- or *y*-Axis in the Rotating Frame

U	$\exp(-i\pi/2I_x)U\ \exp(i\pi/2I_x)$	$\exp(-i\pi/2I_y)U\ \exp(i\pi/2I_y)$
$\hat{T}_{10}$	$-i\hat{T}_{11}(s)$	$-\hat{T}_{11}(a)$
$\hat{T}_{11}(a)$	$\hat{T}_{11}(a)$	$\hat{T}_{10}$
$\hat{T}_{11}(s)$	$-i\hat{T}_{10}$	$\hat{T}_{11}(s)$
$\hat{T}_{20}$	$-1/2\hat{T}_{20} - 1/2\sqrt{3}\ \hat{T}_{22}(s)$	$-1/2\hat{T}_{20} + 1/2\sqrt{3}\ \hat{T}_{22}(s)$
$\hat{T}_{21}(a)$	$-i\hat{T}_{22}(a)$	$-\hat{T}_{21}(a)$
$\hat{T}_{21}(s)$	$-\hat{T}_{21}(s)$	$-\hat{T}_{22}(a)$
$\hat{T}_{22}(a)$	$-i\hat{T}_{21}(a)$	$\hat{T}_{21}(s)$
$\hat{T}_{22}(s)$	$-1/2\sqrt{3}\ \hat{T}_{20} + 1/2\hat{T}_{22}(s)$	$1/2\sqrt{3}\ \hat{T}_{20} + 1/2\hat{T}_{22}(s)$
$\hat{T}_{30}$	$i/2\sqrt{3/2}\ \hat{T}_{31}(s) + i/2\sqrt{5/2}\ \hat{T}_{33}(s)$	$1/2\sqrt{3/2}\ \hat{T}_{31}(a) - 1/2\sqrt{5/2}\ \hat{T}_{33}(a)$
$\hat{T}_{31}(a)$	$-1/4\hat{T}_{31}(a) - 1/4\sqrt{15}\ \hat{T}_{33}(a)$	$-1/2\sqrt{3/2}\ \hat{T}_{30} + 1/2\sqrt{5/2}\ \hat{T}_{32}(s)$
$\hat{T}_{31}(s)$	$i/2\sqrt{3/2}\ \hat{T}_{30} + i/2\sqrt{5/2}\ \hat{T}_{32}(s)$	$-1/4\hat{T}_{31}(s) + 1/4\sqrt{15}\ \hat{T}_{33}(s)$
$\hat{T}_{32}(a)$	$-\hat{T}_{32}(a)$	$-\hat{T}_{32}(a)$
$\hat{T}_{32}(s)$	$i/2\sqrt{5/2}\ \hat{T}_{31}(s) - i/2\sqrt{3/2}\ \hat{T}_{33}(s)$	$-1/2\sqrt{5/2}\ \hat{T}_{31}(a) - 1/2\sqrt{3/2}\ \hat{T}_{33}(a)$
$\hat{T}_{33}(a)$	$-1/4\sqrt{15}\ \hat{T}_{31}(a) + 1/4\hat{T}_{33}(a)$	$1/2\sqrt{5/2}\ \hat{T}_{30} + 1/2\sqrt{3/2}\ \hat{T}_{32}(s)$
$\hat{T}_{33}(s)$	$i/2\sqrt{5/2}\ \hat{T}_{30} - i/2\sqrt{3/2}\ \hat{T}_{32}(s)$	$1/4\sqrt{15}\ \hat{T}_{31}(s) + 1/4\hat{T}_{33}(s)$

$$d\sigma^*/dt = -\int_0^\infty \langle [H^*_{QF}(t), [H^*_{QF}(t-\tau), \sigma^*(t)]]\rangle d\tau \quad [17]$$

With the fluctuating Hamiltonian in Eq. [5], the master equation reads

$$d\sigma^*/dt = -\sum_{m=-2}^{2} [T_{2m}, [T^\dagger_{2m}, \sigma^*]] \times (J_m(m\omega_0) + iK_m(m\omega_0)) \quad [18]$$

with the spectral densities $J_m(m\omega_0)$ and $K_m(m\omega_0)$ being the real and imaginary part of the Fourier transform of the EFG correlation function

$$J_m(\omega) = (eQ/\hbar)^2 \mathrm{Re} \int_0^\infty \langle [F^*_{2m}(t) - \langle F^*_{2m}\rangle] \times [F_{2m}(t-\tau) - \langle F_{2m}\rangle]\rangle \exp(i\omega\tau) d\tau$$

$$K_m(\omega) = (eQ/\hbar)^2 \mathrm{Im} \int_0^\infty \langle [F^*_{2m}(t) - \langle F^*_{2m}\rangle] \times [F_{2m}(t-\tau) - \langle F_{2m}\rangle]\rangle \exp(i\omega\tau) d\tau \quad [19]$$

It should be noticed that in an isotropic environment the average EFG $\langle F_{2m}\rangle = 0$; it has been included here for ease of reference. The imaginary part $K_m(m\omega_0)$ results in a very small shift in the energy of the system and is commonly included (for $I < 3/2$) in a redefined Zeeman Hamiltonian and thus dropped from the relaxation term. However, in the spin $I = 3/2$ manifold, the dynamic shift differs for the central and outer energy level transitions. Accordingly, the general line shape pertaining to the single-quantum coherences consists of a sum of two Lorentzians. Outside the extreme narrowing limit, each Lorentzian has a different width and amplitude, and they are separated by a dynamic frequency shift. Generally, the dynamic shift is too small for experimental observation and it is neglected in most application studies.

With an exponential correlation function with correlation time τ_c, the spectral density function takes the form

$$J_m(\omega) = \frac{(2\pi)^2}{20}\left(\frac{\chi^2\tau_c}{1+\omega^2\tau_c^2}\right) \quad K_m(\omega) = \omega\tau J_m(\omega) \quad [20]$$

where χ denotes the root-mean-square coupling constant. In soft condensed matter, including biological systems, often, there are several independent processes at different timescales causing the loss of correlation. In this case, the spectral density function can be expressed as a sum of Lorentzians; each contribution is characterized by a correlation time and a coupling constant. For a full, model-free

analysis of the spectral density function, it is necessary to do multiple relaxation rate measurements at various Larmor frequencies through variation of the Zeeman field strength.

Subsequently, the density operator is expanded into the irreducible tensor operator basis. Because of the symmetry properties of the double commutator in the relaxation superoperator in Eq. [18], this expansion yields a set of equations in which the subsets pertaining to the various coherence orders are decoupled. Accordingly, under relaxation, the coherence order is conserved, whereas the rank can change. Another symmetry property of the double commutator is that the even and odd rank tensor operators are decoupled, irrespective of the spin quantum number. Initially, the density operator is always in an odd rank-one state (proportional to longitudinal magnetization $\hat{T}_{10}$) and, accordingly, rank-two coherence can never be created by relaxation or by coherence transfer. As we will see in the following section, this rule of thumb no longer applies in the presence of a static quadrupolar interaction, which is particularly promising from an experimental point of view for the detection of long-range order.

Spin Polarization

The relaxation of the $\hat{T}_{10}$, $\hat{T}_{20}$, and $\hat{T}_{30}$ spin polarization tensors involves the dynamics of the eigenstate populations. In the present formalism, the corresponding master equation in Eq. [18] reads

$$\frac{d}{dt}\begin{pmatrix}\hat{T}_{10}\\ \hat{T}_{30}\end{pmatrix} = -\begin{pmatrix}2/5J_1 + 8/5J_2 & 4/5(J_1 - J_2)\\ 4/5(J_1 - J_2) & 8/5J_1 + 2/5J_2\end{pmatrix}\begin{pmatrix}\hat{T}_{10}\\ \hat{T}_{30}\end{pmatrix}, \quad [21]$$

which can be diagonalized and subsequently integrated in analytical form. In the arrow notation (*20*), the solution is given by

$$\hat{T}_{10} \xrightarrow{R^{(0)}} \hat{T}_{10} f_{11}^{(0)}(t) + \hat{T}_{30} f_{31}^{(0)}(t)$$

$$\hat{T}_{30} \xrightarrow{R^{(0)}} \hat{T}_{30} f_{33}^{(0)}(t) + \hat{T}_{10} f_{13}^{(0)}(t) \quad [22]$$

with the biexponential relaxation functions

$$f_{11}^{(0)} = 1/5[\exp(-R_1^{(0)}t) + 4\exp(-R_2^{(0)}t)]$$

$$f_{13}^{(0)} = f_{31}^{(0)} = 2/5[\exp(-R_1^{(0)}t) - \exp(-R_2^{(0)}t)]$$

$$f_{33}^{(0)} = 1/5[4\exp(-R_1^{(0)}t) + \exp(-R_2^{(0)}t)] \quad [23]$$

and rates

$$R_1^{(0)} = 2J_1 \quad R_2^{(0)} = 2J_2 \quad [24]$$

where the superscript (0) denotes longitudinal relaxation (zero quantum) and $J_1 = J_1(\omega_0)$ and $J_2 = J_2(2\omega_0)$. A differential equation describing the coupling of longitudinal magnetization ($\hat{T}_{10} = 1/\sqrt{5}I_z$) and octopolar spin polarization ($\hat{T}_{30}$) was first reported almost 50 years ago by François Lurçat (*21*). Furthermore, this author first showed that the spin-lattice relaxation is biexponential with two relaxation times, provided the fluctuating quadrupolar interactions are outside the extreme narrowing limit (*22*). In 1986, it was realized that the octopolar spin polarization is convertible into multiquantum coherence by a hard RF pulse, which provided a new method for the measurement of multiexponential quadrupolar relaxation (*20*). In the extreme narrowing limit $\omega_0\tau_c \ll 1$ and $J_1 = J_2$, the longitudinal relaxation becomes monoexponential with $R_1^{(0)} = R_2^{(0)}$ and the octopolar spin polarization is no longer created.

The even-rank quadrupolar spin polarization is decoupled from any other tensor operator

$$\frac{d}{dt}\hat{T}_{20} = -(2J_1 + 2J_2)\hat{T}_{20} \quad [25]$$

and its time evolution takes the form

$$\hat{T}_{20} \xrightarrow{R^{(0)}} \hat{T}_{20} f_{22}^{(0)}(t), \quad f_{22}^{(0)} = \exp(-R_3^{(0)}t) \quad [26]$$

with rate

$$R_3^{(0)} = 2J_1 + 2J_2 \quad [27]$$

In an isotropic environment, the quadrupolar spin polarization can not be created by coherence transfer or relaxation and the corresponding rate is inaccessible.

Single-Quantum

McLachlan reported biexponential transverse relaxation of the spin-3/2 electron spin resonance quartet state as early as 1964 (*23*). Expressions for multiexponential nuclear magnetic relaxation for quadrupolar nuclei were given first by Hubbard (*24*). The corresponding master equation for the odd rank tensor operators takes the form

$$\frac{d}{dt}\begin{pmatrix}\hat{T}_{1\pm1}\\ \hat{T}_{3\pm1}\end{pmatrix} = -\begin{pmatrix}1/5(3J_0 + 5J_1 + 2J_2 \pm i(K_1 + 2K_2)) & \sqrt{6}/5(J_0 - J_2 \pm i(2K_1 - K_2))\\ \sqrt{6}/5(J_0 - J_2 \pm i(2K_1 - K_2)) & 1/5(2J_0 + 5J_1 + 3J_2 \mp i(K_1 - 3K_2))\end{pmatrix}\begin{pmatrix}\hat{T}_{1\mp1}\\ \hat{T}_{3\mp1}\end{pmatrix} \quad [28]$$

with solution

$$\hat{T}_{1\pm1} \xrightarrow{R^{(1)}} \hat{T}_{1\pm1}f_{11}^{(\pm1)}(t) + \hat{T}_{3\pm1}f_{31}^{(\pm1)}(t)$$

$$\hat{T}_{3\pm1} \xrightarrow{R^{(1)}} \hat{T}_{1\pm1}f_{13}^{(\pm1)}(t) + \hat{T}_{3\pm1}f_{33}^{(\pm1)}(t) \quad [29]$$

The relaxation functions are biexponential

$$f_{11}^{(\pm1)} = 1/5[3\ \exp(-R_1^{(\pm1)}t) + 2\ \exp(-R_2^{(\pm1)}t)]$$

$$f_{13}^{(\pm1)} = f_{31}^{(\pm1)} = \sqrt{6}/5[\exp(-R_1^{(\pm1)}t) - \exp(-R_2^{(\pm1)}t)]$$

$$f_{33}^{(\pm1)} = 1/5[2\ \exp(-R_1^{(\pm1)}t) + 3\ \exp(-R_2^{(\pm1)}t)] \quad [30]$$

with relaxation eigenvalues

$$R_1^{(\pm1)} = J_0 + J_1 \pm iK_1$$

$$R_2^{(\pm1)} = J_1 + J_2 \mp i(K_1 - K_2) \quad [31]$$

It should be noticed that the transverse relaxation is particularly sensitive to slow molecular motion through the spectral density at zero frequency $J_0(0) = J_0$. In the presence of a low-frequency dispersion in the spectral density, the relaxation of the rank-one and rank-three single-quantum coherences is biexponential. Furthermore, as in the case of the eigenstate population dynamics, the creation of the rank-three coherence allows for the excitation of multiple-quantum coherence with the help of a coherence transfer pulse (*20, 25*). In the extreme narrowing limit, the transverse relaxation is monoexponential and the rank-three coherence is no longer created.

The fast and the slowly relaxing components with relaxation eigenvalues $R_1^{(\pm1)}$ and $R_2^{(\pm1)}$ are dynamically shifted with respect to the Larmor frequency with shifts K_1 and $K_2 - K_1$, respectively. Accordingly, the spectra resulting from Fourier transformation of the relaxation functions are generally a sum of two Lorentzians separated by the difference of the dynamic shifts pertaining to the central and outer transitions of the spin-3/2 manifold $2K_1$-K_2 (*26, 27*). In practice, this dynamic shift usually is much smaller than the line widths and notoriously difficult to detect (*28, 29*).

In an isotropic environment, the rank-two single-quantum coherence is decoupled from any other tensor operator and, accordingly, its rate is inaccessible. For the sake of completeness, we give the corresponding differential equation

$$\frac{d}{dt}\hat{T}_{2\pm1} = -(J_0 + J_1 + 2J_2 \pm iK_1)\hat{T}_{2\pm1} \quad [32]$$

and its time evolution takes the form

$$\hat{T}_{2\pm1} \xrightarrow{R^{(1)}} \hat{T}_{2\pm1}f_{22}^{(\pm1)}(t)$$

$$f_{22}^{(\pm1)} = \exp(-R_3^{(\pm1)}t) \quad [33]$$

with relaxation eigenvalue

$$R_3^{(\pm1)} = J_0 + J_1 + 2J_2 \mp iK_1 \quad [34]$$

Here, the dynamic shift can be included in a redefined Zeeman Hamiltonian and dropped from the relaxation term.

The difference in time evolution of the positive and negative coherence orders is seen to vanish if the dynamic frequency shifts K_1 and K_2 are neglected. With this approximation, the symmetric and antisymmetric tensor combinations are decoupled

$$\hat{T}_{11}(s, a) \xrightarrow{R^{(1)}} \hat{T}_{11}(s, a)f_{11}^{(1)}(t) + \hat{T}_{31}(s, a)f_{31}^{(1)}(t)$$

$$\hat{T}_{31}(s, a) \xrightarrow{R^{(1)}} \hat{T}_{11}(s, a)f_{13}^{(1)}(t) + \hat{T}_{31}(s, a)f_{33}^{(1)}(t) \quad [35]$$

for the observable coherences and

$$\hat{T}_{21}(s, a) \xrightarrow{R^{(1)}} \hat{T}_{21}(s, a)f_{22}^{(1)}(t) \quad [36]$$

for the inaccessible rank-two single-quantum coherences. The relaxation functions are given by Eqs. [30] and [33] with rates

$$R_1^{(1)} = J_0 + J_1$$
$$R_2^{(1)} = J_1 + J_2$$
$$R_3^{(1)} = J_0 + J_1 + 2J_2 \qquad [37]$$

where the $\pm$ sign in the superscript has been dropped to express the equality of the dynamics of the positive and negative coherence orders.

Multiple Quantum

The double-quantum and triple-quantum coherences relax independently according to single exponentials. As in the case of the rank-two, single-quantum coherence, caused by the symmetry of the spin-3/2 manifold, the dynamic shifts can be included in a redefined Zeeman Hamiltonian and thus dropped from the relaxation terms. The rank-two and rank-three double-quantum coherences relax independently and their time evolution takes the form

$$\hat{T}_{22}(s, a) \xrightarrow{R^{(2)}} \hat{T}_{22}(s, a) f_{22}^{(2)}(t)$$
$$\hat{T}_{32}(s, a) \xrightarrow{R^{(2)}} \hat{T}_{32}(s, a) f_{33}^{(2)}(t) \qquad [38]$$

with evolution functions

$$f_{22}^{(2)} = \exp(-R_1^{(2)} t)$$
$$f_{33}^{(2)} = \exp(-R_2^{(2)} t) \qquad [39]$$

and rates

$$R_1^{(2)} = J_0 + 2J_1 + J_2$$
$$R_2^{(2)} = J_0 + J_2 \qquad [40]$$

It should be noticed that the rate $R_1^{(2)}$ pertaining to the rank-two double-quantum coherence is inaccessible.

For the triple-quantum coherence, the time evolution can be derived analogously and the solution reads

$$\hat{T}_{33}(s, a) \xrightarrow{R^{(3)}} \hat{T}_{33}(s, a) f_{33}^{(3)}(t)$$
$$f_{33}^{(3)} = \exp(-R_1^{(3)} t)$$
$$R_1^{(3)} = J_1 + J_2 \qquad [41]$$

THERMAL RELAXATION IN AN ANISOTROPIC ENVIRONMENT

So far, the formalism is strictly valid for nuclei in an isotropic environment, where the nuclei experience a zero-average EFG. In many important systems, including biological tissue and lyotropic liquid crystals, the quadrupolar interaction is not completely averaged by molecular motion in times less than the inverse Larmor frequency and the nuclear magnetic resonance (NMR) spectra display residual, possibly hidden, quadrupolar splitting. Accordingly, to extend the range of applications to this important class of materials, it is necessary to include the static quadrupolar Hamiltonian in the calculation of the evolution of the density operator. In the absence of an RF field, the static Hamiltonian $H_S^* = H_{QS}^*$ commutes with $H_{QF}^*(t)$ and, accordingly, vanishes in the relaxation superoperator in Eq. [8]. In the rotating frame, the time dependence of the density operator now reads

$$d\sigma^*/dt = -i\omega_Q/\sqrt{6}\,[T_{20}, \sigma^*] - \sum_{m=-2}^{2} [T_{2m}, [T_{2m}^\dagger, \sigma^*]] \times (J_m(m\omega_0) + iK_m(m\omega_0)) \qquad [42]$$

In the expansion of the density operator into the irreducible tensor operator basis, the subsets pertaining to different coherence orders are still decoupled. However, as we will see, because of the evolution under the static quadrupolar Hamiltonian, the decoupling of the odd and even rank tensor operators is lifted. This phenomenon allows for the creation of rank-two coherence, which provides for a unique experimental method to probe the existence of long-range order.

Spin Polarization

Longitudinal relaxation involves the dynamics of the eigenstate populations. The corresponding zero-order tensor operators (i.e., the diagonal elements of the density operator) commute with the static quadrupolar Hamiltonian and, hence, the first term on the right side of Eq. [42] is identically zero. The resulting sets of coupled differential equations are the same as the ones for spin 3/2 in the isotropic environment and their solutions are given by Eqs. [22] and [26].

Single Quantum

In contrast to the eigenstate population dynamics, a static field gradient has a profound effect on the evolution of the nonzero quantum coherences. For the sake of simplicity, we ignore the dynamic frequency shifts. Including the static quadrupolar Hamiltonian, the master equation pertaining to the single-quantum coherences takes the form

$$\frac{d}{dt}\begin{pmatrix}\hat{T}_{11}(a,s)\\ \hat{T}_{21}(s,a)\\ \hat{T}_{31}(a,s)\end{pmatrix} = -\begin{pmatrix}3/5J_0 + J_1 + 2/5J_2 & -i\sqrt{3/5}\omega_Q & \sqrt{6}/5(J_0 - J_2)\\ -i\sqrt{3/5}\omega_Q & J_0 + J_1 + 2J_2 & -i\sqrt{2/5}\omega_Q\\ \sqrt{6}/5(J_0 - J_2) & -i\sqrt{2/5}\omega_Q & 2/5J_0 + J_1 + 3/5J_2\end{pmatrix}\begin{pmatrix}\hat{T}_{11}(a,s)\\ \hat{T}_{21}(s,a)\\ \hat{T}_{31}(a,s)\end{pmatrix} \quad [43]$$

where the odd and even rank tensor operators are now seen to be coupled. These differential equations can be integrated in analytical form (*30*) and the resulting time dependencies read

$$\hat{T}_{11}(a,s) \xrightarrow{R^{(1)}} \hat{T}_{11}(a,s) f_{11}^{(1)}(t) + \hat{T}_{21}(s,a) f_{21}^{(1)}(t) + \hat{T}_{31}(a,s) f_{31}^{(1)}(t)$$

$$\hat{T}_{21}(s,a) \xrightarrow{R^{(1)}} \hat{T}_{11}(a,s) f_{12}^{(1)}(t) + \hat{T}_{21}(s,a) f_{22}^{(1)}(t) + \hat{T}_{31}(a,s) f_{32}^{(1)}(t)$$

$$\hat{T}_{31}(a,s) \xrightarrow{R^{(1)}} \hat{T}_{11}(a,s) f_{13}^{(1)}(t) + \hat{T}_{21}(s,a) f_{23}^{(1)}(t) + \hat{T}_{31}(a,s) f_{33}^{(1)}(t) \quad [44]$$

with the evolution functions

$$\begin{aligned}
f_{11}^{(1)} &= 1/5[3/2(1 + J_2/(J_2^2 - \omega_Q^2)^{1/2})\exp(-R_1^{(1)}t) + 2\exp(-R_2^{(1)}t) + 3/2(1 - J_2/(J_2^2 - \omega_Q^2)^{1/2}\exp(-R_3^{(1)}t)]\\
f_{12}^{(1)} &= f_{21}^{(1)} = i/2\sqrt{3/5}\,\omega_Q/(J_2^2 - \omega_Q^2)^{1/2}[\exp(-R_1^{(1)}t) - \exp(-R_3^{(1)}t)]\\
f_{13}^{(1)} &= f_{31}^{(1)} = \sqrt{6}/5[1/2(1 + J_2/(J_2^2 - \omega_Q^2)^{1/2})\exp(-R_1^{(1)}t) - \exp(-R_2^{(1)}t) + 1/2(1 - J_2/(J_2^2 - \omega_Q^2)^{1/2})\exp(-R_3^{(1)}t)]\\
f_{22}^{(1)} &= 1/2[(1 - J_2/(J_2^2 - \omega_Q^2)^{1/2})\exp(-R_1^{(1)}t) + (1 + J_2/(J_2^2 - \omega_Q^2)^{1/2})\exp(-R_3^{(1)}t)]\\
f_{23}^{(1)} &= f_{32}^{(1)}(t) = i/\sqrt{10}\,\omega_Q/(J_2^2 - \omega_Q^2)^{1/2}[\exp(-R_1^{(1)}t) - \exp(-R_3^{(1)}t)]\\
f_{33}^{(1)} &= 1/5[(1 + J_2/(J_2^2 - \omega_Q^2)^{1/2})\exp(-R_1^{(1)}t) + 3\exp(-R_2^{(1)}t) + (1 - J_2/(J_2^2 - \omega_Q^2)^{1/2})\exp(-R_3^{(1)}t)]
\end{aligned} \quad [45]$$

and relaxation eigenvalues

$$\begin{aligned}
R_1^{(1)} &= J_0 + J_1 + J_2 - (J_2^2 - \omega_Q^2)^{1/2}\\
R_2^{(1)} &= J_1 + J_2\\
R_3^{(1)} &= J_0 + J_1 + J_2 + (J_2^2 - \omega_Q^2)^{1/2}
\end{aligned} \quad [46]$$

For $\omega_Q = 0$, these expressions reduce to the ones pertaining to the isotropic environment. If the dynamic shifts are included, the symmetric and antisymmetric tensor combinations are coupled and the outer and central transitions are shifted with frequencies K_1 and K_2-K_1, respectively, as in the isotropic environment.

Two regimes in the single-quantum eigensystem can be distinguished as $\omega_Q > J_2$ and $\omega_Q < J_2$, respectively. In the range of $\omega_Q < J_2$, the relaxation eigenvalues in Eq. [46] are real and line splitting is absent, despite the presence of a non–zero-average EFG. The conventional single-quantum spectra, i.e., the Fourier transforms of the time evolutions involv-

ing the odd rank tensor operators $f_{11}^{(1)}, f_{13}^{(1)} = f_{31}^{(1)}$, and $f_{33}^{(1)}$, consist of a sum of three Lorentzians. The widths and relative (real) amplitudes of these components are sensitive to the value of ω_Q and are experimentally difficult to fit. However, a promising feature, which is suitable for fitting, is the creation of rank-two coherences if $\omega_Q \neq 0$. The evolution from rank-one or rank-three into rank-two tensor operators $f_{12}^{(1)} = f_{21}^{(1)}$ and $f_{32}^{(1)} = f_{23}^{(1)}$, respectively, is always biexponential with equal amplitude fractions but opposite signs. Two different pulse sequences to detect selectively rank-two tensor coherences will be discussed.

If $\omega_Q > J_2$, the relaxation eigenvalues $R_1^{(1)}$ and $R_3^{(1)}$ in Eq. [46] pertaining to the outer transitions of the spin-3/2 manifold are complex and the satellite transitions are shifted by $\pm(\omega_Q^2 - J_2^2)^{1/2}$ with respect to the central line. If the dynamic shifts are included, the splitting takes the values $\pm(\omega_Q^2 - J_2^2)^{1/2} - 2K_1 + K_2$ and the spectrum becomes asymmetric. The line widths given by the real part of the relaxation eigenvalues are now insensitive to the value of ω_Q. The satellites in the Fourier transforms of the relaxation functions $f_{11}^{(1)}$, $f_{13}^{(1)} = f_{31}^{(1)}$, and $f_{33}^{(1)}$ have complex amplitudes and, hence, they are (symmetrically) phase twisted with respect to the central line. For small values of ω_Q, but for $\omega_Q > J_2$, splitting of the resonance may be unobservable if the static quadrupolar interaction does not exceed the line widths. In the latter situation, rank-two coherence order is still created, which can be used to detect the existence of a hidden static quadrupolar coupling.

For large splitting $\omega_Q \gg J_2$, the satellite signals no longer overlap with the central transition and the relaxation functions in Eq. [45] take to a very good approximation the form (*31*)

$$
\begin{aligned}
f_{11}^{(1)} &= 1/5[3/2\ \exp(-(R_s^{(1)} - i\omega_Q)t) + 2\ \exp(-R_c^{(1)}t) + 3/2\ \exp(-(R_s^{(1)} + i\omega_Q)t)] \\
f_{12}^{(1)} &= f_{21}^{(1)} = 1/2\sqrt{3/5}\ [\exp(-(R_s^{(1)} - i\omega_Q)t) - \exp(-(R_s^{(1)} + i\omega_Q)t)] \\
f_{13}^{(1)} &= f_{31}^{(1)} = \sqrt{6}/5[1/2\ \exp(-(R_s^{(1)} - i\omega_Q)t) - \exp(-R_c^{(1)}t) + 1/2\ \exp(-(R_s^{(1)} + i\omega_Q)t)]_{\omega_Q \gg J_2} \\
f_{22}^{(1)} &= 1/2[\exp(-(R_s^{(1)} - i\omega_Q)t) + \exp(-(R_s^{(1)} + i\omega_Q)t)] \\
f_{23}^{(1)} &= f_{32}^{(1)}(t) = 1/\sqrt{10}[\exp(-(R_s^{(1)} - i\omega_Q)t) - \exp(-(R_s^{(1)} + i\omega_Q)t)] \\
f_{33}^{(1)} &= 1/5[\exp(-(R_s^{(1)} - i\omega_Q)t) + 3\ \exp(-R_c^{(1)}t) + \exp(-(R_s^{(1)} + i\omega_Q)t)]
\end{aligned}
\qquad [47]
$$

with the relaxation rates of the satellites and central transition, respectively,

$$
\begin{aligned}
R_s^{(1)} &= J_0 + J_1 + J_2 \\
R_c^{(1)} &= J_1 + J_2
\end{aligned}
\qquad [48]
$$

As can be seen in Eq. [47], the satellites are either in the same phase ($f_{11}^{(1)}, f_{33}^{(1)}$) or in antiphase ($f_{13}^{(1)} = f_{31}^{(1)}$) with the central transition. Note that in the presence of a static quadrupolar interaction, the rate pertaining to the satellite signal $R_s^{(1)} = J_0 + J_1 + J_2$ differs from the one pertaining to the fast transverse relaxation mode in the isotropic environment $R_1^{(1)} = J_0 + J_1$ (Eq. [37]). Furthermore, the satellite signals are liable to line broadening because of the possible presence of an inhomogeneous distribution in static quadrupolar interaction through the sample, which makes an accurate measurement of the natural line width difficult, if not impossible. A method to eliminate effectively this inhomogeneous line broadening effect will be discussed.

Multiple Quantum

As in an isotropic environment, for the multiple-quantum coherences, the dynamic shifts can be included in a redefined Zeeman Hamiltonian and dropped from the relaxation term. The double-quantum rank-two and rank-three coherences are now coupled by the static quadrupolar interaction and the corresponding master equation reads

$$\frac{d}{dt}\begin{pmatrix}\hat{T}_{22}(s,\,a)\\ \hat{T}_{32}(a,\,s)\end{pmatrix} = -\begin{pmatrix}J_0 + 2J_1 + J_2 & -i\omega_Q\\ -i\omega_Q & J_0 + J_2\end{pmatrix} \times \begin{pmatrix}\hat{T}_{22}(s,\,a)\\ \hat{T}_{32}(a,\,s)\end{pmatrix} \quad [49]$$

with solution

$$\hat{T}_{22}(s,\,a) \xrightarrow{R^{(2)}} \hat{T}_{22}(s,\,a)\,f_{22}^{(2)}(t) + \hat{T}_{32}(a,\,s)\,f_{32}^{(2)}(t)$$

$$\hat{T}_{32}(a,\,s) \xrightarrow{R^{(2)}} \hat{T}_{22}(s,\,a)\,f_{23}^{(2)}(t) + \hat{T}_{33}(a,\,s)\,f_{33}^{(2)}(t) \quad [50]$$

The relaxation functions take the form

$$\begin{aligned} f_{22}^{(2)} &= 1/2[(1 + J_1/(J_1^2 - \omega_Q^2)^{1/2})\exp(-R_1^{(2)}t) \\ &\quad + (1 - J_1/(J_1^2 - \omega_Q^2)^{1/2})\exp(-R_2^{(2)}t)] \\ f_{23}^{(2)} &= f_{32}^{(2)} = -i/2\omega_Q/(J_1^2 - \omega_Q^2)^{1/2} \\ &\quad [\exp(-R_1^{(2)}t) - \exp(-R_2^{(2)}t)] \\ f_{33}^{(2)} &= 1/2[(1 - J_1/(J_1^2 - \omega_Q^2)^{1/2})\exp(-R_1^{(2)}t) + \\ &\quad (1 + J_1/(J_1^2 - \omega_Q^2)^{1/2})\exp(-R_2^{(2)}t)] \end{aligned} \quad [51]$$

with relaxation eigenvalues

$$\begin{aligned} R_1^{(2)} &= J_0 + J_1 + J_2 + (J_1^2 - \omega_Q^2)^{1/2} \\ R_2^{(2)} &= J_0 + J_1 + J_2 - (J_1^2 - \omega_Q^2)^{1/2} \end{aligned} \quad [52]$$

As in the case of the single-quantum eigensystem, for the double-quantum coherences, two regimes can be distinguished $\omega_Q > J_1$ and $\omega_Q < J_1$, respectively (notice that the critical value is now J_1 instead of J_2). In the range $\omega_Q < J_1$, the relaxation eigenvalues in Eq. [52] are real and line splitting is not observed. The spectra pertaining to the relaxation of the double-quantum coherences consist of a sum of two Lorentzians. If $\omega_Q > J_1$, the relaxation eigenvalues are complex and two satellites in (twisted) antiphase are observed at frequencies $\pm(\omega_Q^2 - J_1^2)^{1/2}$ with respect to the Larmor frequency. The line width is given by the real part of the relaxation eigenvalues and is the same as the one pertaining to the satellites in the single-quantum spectra.

The relaxation dynamics of the triple-quantum coherences is unaffected by the static quadrupolar coupling.

PULSE SEQUENCES

Longitudinal Relaxation

The measurement of the spectral density at one and two times the Larmor frequency is most conveniently facilitated by an inversion recovery experiment. In this experiment, a nonselective (π) pulse is applied to invert the magnetization. After this initial pulse, the deviation of the density operator from thermal equilibrium reads

$$\Delta\sigma^*(t = 0) = -2I_z = -2\sqrt{5}\hat{T}_{10} \quad [53]$$

After the preparation pulse, the density operator evolves back toward equilibrium according to Eq. [22]. To obtain the density operator as a function of the evolution time t_1, one has to add the equilibrium value

$$\begin{aligned} \sigma^*(t_1) &= \Delta\sigma^*(t_1) + I_z \\ &= \sqrt{5}\,[\hat{T}_{10}(1 - 2f_{11}^{(0)}(t_1)) - 2\hat{T}_{30}f_{31}^{(0)}(t_1)] \end{aligned} \quad [54]$$

After partial recovery a $(\pi/2)_y$ readout pulse is given. With the results in Table 3, the density operator is now represented by a sum of single- and triple-quantum coherences

$$\begin{aligned} \sigma^*(t_1) &= \sigma^*(t_1,\,p = 1) + \sigma^*(t_1,\,p = 3) \\ \sigma^*(t_1,\,p = 1) &= \sqrt{5}\,[\hat{T}_{11}(a)(1 - 2f_{11}^{(0)}(t_1)) \\ &\quad + \sqrt{3/2}\,\hat{T}_{31}(a)\,f_{31}^{(0)}(t_1)] \\ \sigma^*(t_1,\,p = 3) &= -5/\sqrt{2}\,\hat{T}_{33}(a)f_{31}^{(0)}(t_1) \end{aligned} \quad [55]$$

Under direct detection, the signal is proportional to the single-quantum ($p = 1$) coherence contribution and reads

$$\begin{aligned} s(t_1,\,t_2) &= (1 - 2f_{11}^{(0)}(t_1))\,f_{11}^{(1)}(t_2) \\ &\quad + \sqrt{3/2}\,f_{31}^{(0)}(t_1)\,f_{13}^{(1)}(t_2)\ (T_1 \text{ relaxation}) \end{aligned} \quad [56]$$

The second term on the right side comes from the rank-three single-quantum coherence, which evolves back into observable magnetization during the acquisition period. The effect of this interference term can be minimized by recording the amplitude of the detected signal right after the readout pulse, or, alternatively, by integrating the entire spectrum after Fourier transformation of the FID. Another option is to decrease the readout pulse angle to the value arc

$\cos(1/\sqrt{5}) = 63.4°$, so that the transfer of $\hat{T}_{30}$ into $\hat{T}_{31}(a)$ is exactly nullified (*32*).

In an anisotropic system, it is of interest to identify the individual longitudinal relaxation of the satellites and central transition, respectively. For this purpose, the relaxation functions in Eq. [56] are expanded and the time evolution takes the form

$$s(t_1, t_2) = 3/5[1 - 2\exp(-R_2^{(0)}t_1)] \times [\exp(-(R_s^{(1)} - i\omega_Q)t_2) + \exp(-(R_s^{(1)} + i\omega_Q)t_2)] + 2/5[1 - [\exp(-R_1^{(0)}t_1) + \exp(-R_2^{(0)}t_1)]]\exp(-R_2^{(1)}t_2) \quad [57]$$

Without loss of generality, we have used the limiting expression in Eq. [47] pertaining to the situation with large quadrupolar splitting $\omega_Q \gg J_2$. After Fourier transformation with respect to the acquisition time t_2 (F_2 domain), a set of spectra is obtained. The first term on the right side of Eq. [57] is readily identified as the satellite contribution, which relaxes according to a single exponential with rate $R_2^{(0)}$ in the evolution period t_1. The longitudinal relaxation of the central line (the second term) is biexponential with equal fractions and rates $R_1^{(0)}$ and $R_2^{(0)}$, respectively (*31*). In practice, biexponential longitudinal relaxation of the central line is difficult to detect, because the difference in the two relaxation modes generally is small. However, a difference in longitudinal relaxation behavior between the satellites and central transition is a convenient tool to detect dispersion in the Larmor frequency range.

A critical and convenient experiment for the detection of high-frequency dispersion in the spectral density is provided by a combination of the inversion recovery experiment with a triple-quantum filter (TQF)

$$\pi(0) - \text{evolution}, t_1 - \pi/2(\phi) - \text{mixing}, t_m - \pi/2(0) - \text{acquire}, t_2. \quad [58]$$

The phase ϕ is stepped through the values 30, 90, 150, 210, 270, and 330°, while the receiver phase is toggled between 0 and 180° for consecutive scans. The mixing time t_m is typically a few microseconds to allow for phase shifting of the pulses. With the transformation properties in Table 3, the TQF signal can be calculated easily

$$s(t_1, t_2, p = 3) = 5/4\sqrt{3/2}\, f_{31}^{(0)}(t_1) f_{13}^{(1)}(t_2) \quad \text{(TQF } T_1 \text{ relaxation)} \quad [59]$$

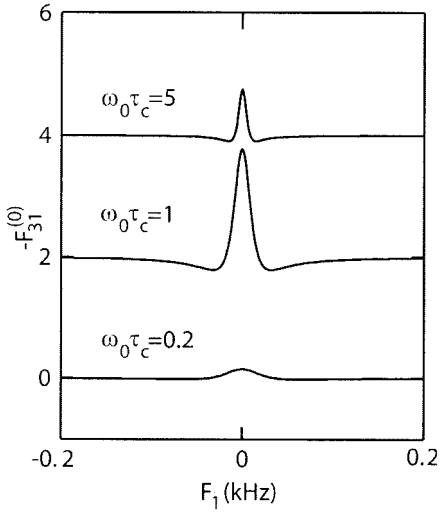

Figure 1 Simulated spectra resulting from the Fourier transform of $f_{31}^{(0)}$ pertaining to the TQF inversion recovery experiment. The spectra are calculated with $\chi = 100$ kHz and $\tau_c = 5$ ns, with a frequency-independent contribution to the spectral density of 25 s^{-1}. The spectra are shifted along the *y*-axis to avoid overlap.

In practice, a set of spectra is obtained after Fourier transformation with respect to the acquisition time t_2. A phase-sensitive 2D spectrum now can be obtained by taking the real part of this set and subsequent Fourier transformation with respect to the evolution time t_1. The signal in the F_1 domain [Fourier transform of $f_{31}^{(0)}(t_1)$] now can be selected by taking a slice along F_1 at the resonance frequency in F_2. Simulated spectra for various values of $\omega_0\tau_c$ are displayed in Fig. 1. Values for the other parameters are chosen in accordance with the experimental results for sodium in DNA solutions, where the spectral density takes the form of a single Lorentzian superposed on a constant (*3*). In the TQF inversion recovery experiment, a noticeable signal is detected only if $\omega_0\tau_c \approx 1$; for $\omega_0\tau_c \ll 1$ and $\omega_0\tau_c \gg 1$ the signal disappears because the spectral density dispersion in the high-frequency region becomes invisibly small.

Transverse Relaxation

Slow dynamics is probed in a transverse relaxation experiment through the spectral density at zero frequency J_0. After an initial ($\pi/2$) pulse, the density operator evolves according to

$$\sigma^*(t_1) = \sqrt{5}\,[\hat{T}_{11}(a) f_{11}^{(1)}(t_1) + \hat{T}_{21}(s) f_{21}^{(1)}(t_1) + \hat{T}_{31}(a) f_{31}^{(1)}(t_1)] \quad [60]$$

In a spin-echo experiment, a $(\pi)_x$ refocusing pulse is applied, which leaves the tensor operator combinations unchanged. The directly detected signal is accordingly represented by

$$s(t_1) = f_{11}^{(1)}(t_1) \ (T_2 \text{ relaxation}) \qquad [61]$$

As in the case of longitudinal relaxation, multiexponential transverse relaxation is conveniently probed with a multiple-quantum filter

$$\pi/2(\phi) - \text{evolution}, t_1/2 - \pi(\phi) - \text{evolution}, t_1/2 - \pi/2(\phi + \phi') - \text{mixing}, t_m - \pi/2(0) - \text{acquire}, t_2 \qquad [62]$$

where the phase ϕ' is 0 and 90° for double and TQF, respectively. The phase ϕ is stepped through the values 30, 90, 150, 210, 270, and 330° for TQF, and through 0, 90, 180, and 270° for double-quantum filtration, while the receiver phase is toggled between 0 and 180° for consecutive scans. The TQF experiment is preferred because it yields 50% greater signal amplitude than the double-quantum filtration experiment (*33*). Furthermore, the double-quantum filtration experiment is more complicated, because both rank-two and rank-three double-quantum coherence $\hat{T}_{22}$ and $\hat{T}_{32}$, respectively, are excited during the mixing period. In the case of the TQF experiment, the second $\pi/2$ pulse converts the created rank-three single-quantum coherence $\hat{T}_{31}$ into triple-quantum coherence. After the mixing time (a few microseconds), the triple-quantum coherence is converted into rank-three single-quantum coherence by the final readout pulse. The rank-three single-quantum coherence evolves into observable magnetization during the acquisition interval. With the transformation properties in Table 3, the corresponding TQF transverse relaxation signal can be calculated easily:

$$s(t_1, t_2, p = 3) = 15/16 f_{31}^{(1)}(t_1) f_{13}^{(1)}(t_2) \ (\text{TQF } T_2 \text{ relaxation}) \qquad [63]$$

where the time evolution during the mixing period has been neglected.

Simulated spectra resulting from the Fourier transform of $f_{31}^{(1)}$ without a static quadrupolar coupling pertaining to nuclei in an isotropic environment are displayed in Fig. 2. Notice that in the TQF transverse relaxation experiment appreciable signal is observed if $\omega_0\tau_c \gtrsim 1$. Accordingly, a great advantage of this experiment is that it is selective for nuclei involved in slow molecular motion, which are characterized by low-frequency dispersion in the spectral density. A signal from nuclei with motional properties in the extreme narrowing limit does not pass the filter. However, the TQF experiment does not discriminate between nuclei in an isotropic and anisotropic environment; the triple-quantum signal is generated irrespective of the presence of a static EFG. In an anisotropic environment with a quadrupolar splitting exceeding the line width, the corresponding spectra show two satellites in antiphase with respect to the central resonance (Fig. 3). Here, the TQF signal is generated irrespective of the motional narrowing conditions and the filter has lost its selectivity to nuclei involved in slow molecular motion.

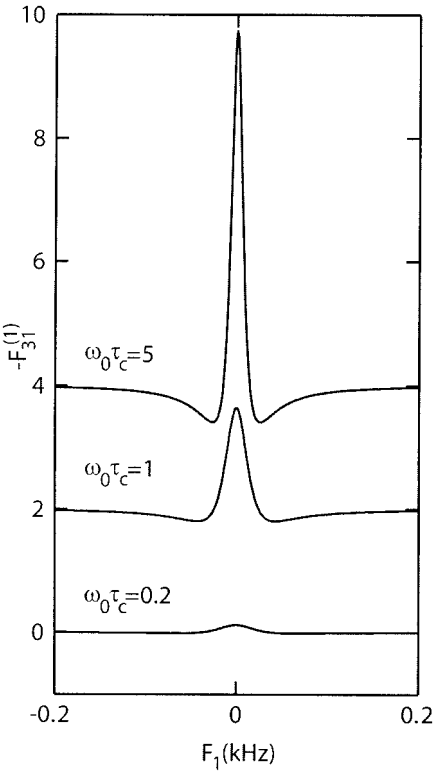

Figure 2 Simulated spectra as in Fig. 1, but for the Fourier transform of $f_{31}^{(1)}$ pertaining to the TQF T_2 relaxation experiment.

Long-Range Order

As has been described, rank-two coherence order is exclusively created in an anisotropic environment where the nuclei experience a non–zero-average EFG. Accordingly, any pulse sequence that selectively detects rank-two coherence order is selective to nuclei in

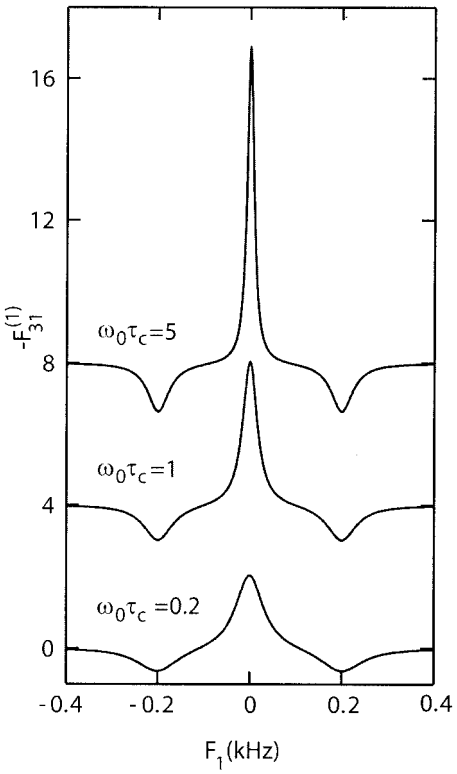

Figure 3 Simulated spectra as in Fig. 1, but for the Fourier transform of $f_{31}^{(1)}$ pertaining to the TQF T_2 relaxation experiment in anisotropic environment with $\omega_Q/2\pi = 200$ Hz.

an ordered environment. As examples, we will discuss the Jeener-Broekaert (JB) and the double-quantum magic-angle (DQ-MA) experiments; for a more extensive review of multiquantum filters and order the reader is referred to Refs. *34* and *35*.

In the JB experiment, the signal is filtered through the spin polarization quadrupolar order $\hat{T}_{20}$ state. The pulse sequence reads

$$\pi/2(\phi) - \text{evolution}, t_1/2 - \pi(\phi) - \text{evolution}, t_1/2 - \pi/4(\phi + 90) - \text{mixing}, t_m - \pi/4(0) - \text{acquire}, t_2 \quad [64]$$

where the phase ϕ is stepped through the values 0, 90, 180, 180, and 270° with constant receiver phase. Unwanted longitudinal $\hat{T}_{10}$ and octopolar spin polarization order $\hat{T}_{30}$ can be suppressed by taking the difference of the slices along F_1 taken at the positive and negative satellite positions in the acquisition domain F_2. Here, the first $\pi/4$ pulse converts the created rank-two single-quantum coherence $\hat{T}_{21}$ into spin polarization quadrupolar order $\hat{T}_{20}$, which is converted back by the final readout pulse. The signal filtered through the $\hat{T}_{20}$ state is calculated easily and takes the form

$$s(t_1, t_2, p = 0) = 3/4 f_{21}^{(1)}(t_1) f_{12}^{(1)} \times (t_2) \quad \text{(JB experiment)} \quad [65]$$

A simulated 2D spectrum pertaining to the JB experiment is shown in Fig. 4. Notice the absence of a central resonance and the two satellites in antiphase in both domains.

Another option is a double-quantum filtered transverse relaxation experiment in which the conversion of the rank-three single-quantum coherence $\hat{T}_{31}$ into double-quantum coherence is suppressed by a judicious choice of the flip angles. In Table 2, it is seen that the transfer of the relevant tensor operator $\hat{T}_{31}(s)$ into rank-three double-quantum coherence $\hat{T}_{32}(s)$ is exactly canceled if the flip angle is decreased to the magic angle arc $\cos(1/\sqrt{3}) = 54.7°$. Cycling through the rank-two double-quantum state $\hat{T}_{22}$ can be affected accordingly by the pulse sequence

$$\pi/2(\phi) - \text{evolution}, t_1/2 - \pi(\phi) - \text{evolution}, t_1/2 - 54.7°(\phi) - \text{mixing}, t_m - 54.7°(0) - \text{acquire}, t_2 \quad [66]$$

where the phase ϕ is stepped through 0, 90, 180, and 270°, while the receiver phase is toggled between 0

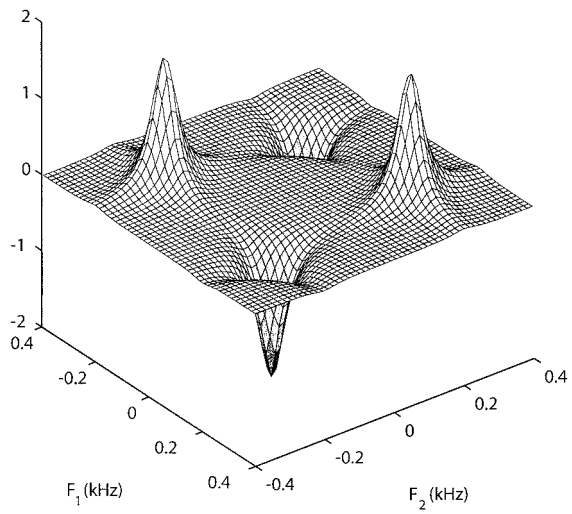

Figure 4 Simulated spectrum pertaining to the JB or DQ-MA experiment with $\omega_Q/2\pi = 200$ Hz and $\omega_0\tau_c = 1$. The other parameters are as in Fig. 1. Notice the two satellites in antiphase in F_1 and F_2 and the absence of the central peak.

and 180° for consecutive scans. The double-quantum filtered spectrum is close to the one pertaining to the JB experiment and the signal reads

$$s(t_1, t_2, p = 2) = 2/3 f_{21}^{(1)}(t_1) f_{12}^{(1)}(t_2)$$

(DQ-MA experiment) [67]

Both the JB and the DQ-MA pulse sequence rely on flip angle and phase effects for the selection of the rank-two signal contributions. Another method, which will be reviewed in part II, is a spin-lock sequence followed by a coherence transfer pulse. This sequence generates spin polarization quadrupolar order and converts it into observable magnetization, when there are residual quadrupolar couplings in the sample and provided the spin-lock field strength is comparable with these couplings. The spin-lock filtering technique does not rely on a flip angle effect for the selection of the desired signal component and therefore might prove preferable in application studies (*36*).

Delayed Acquisition

Satellite signals are liable to line broadening because of the possible presence of an inhomogeneous distribution in static quadrupolar interaction across the sample. This inhomogeneous broadening makes an accurate measurement of the spectral density at zero frequency J_0 in ordered material difficult, if not impossible. Recently, it has been shown that in the case of a powder-type variation of the static quadrupolar coupling, slow dynamics is probed more efficiently by applying a lock through a radio-frequency field (*6*). Another method to effectively eliminate the inhomogeneous broadening is based on delayed acquisition (*37–39*). The most important example of the latter category is the quadrupolar echo (QE) experiment.

The QE experiment is a two $\pi/2$-pulse experiment

$$\pi/2(\phi) - \text{evolution}, t_1/2 - \pi/2(\phi + 90) - \text{evolution}, t_1/2 - \text{acquire}, t_2 \quad [68]$$

where the (primary) echo is formed at a time $\tau = t_1/2$ after the second RF pulse. It should be noticed that the acquisition is delayed and started after the formation of the echo. The signal can be calculated easily with the evolution functions, the definition of the time intervals in Eq. [68], and the transformation properties of the tensor operators in Table 3

$$\begin{aligned} s(t_1, t_2) = {} & f_{11}^{(1)}(t_1/2) f_{11}^{(1)}(t_1/2 + t_2) \\ & - f_{21}^{(1)}(t_1/2) f_{12}^{(1)}(t_1/2 + t_2) \\ & - 1/4 f_{31}^{(1)}(t_1/2) f_{13}^{(1)}(t_1/2 + R_{t_2}) \end{aligned}$$

(QE experiment) [69]

To identify the various signal contributions, the evolution functions are expanded

$$\begin{aligned} s(t_1, t_2) = {} & \\ & \frac{3}{20}\left[-\frac{1}{2}\exp(-(R_s^{(1)} - i\omega_Q)t_1) + \exp(-((R_s^{(1)} + R_c^{(1)})/2 - i\omega_Q/2)t_1) + \frac{3}{2}\exp(-R_s{}^{(1)}t_1)\right]\exp(-(R_s^{(1)} - i\omega_Q)t_2) \\ & + \frac{1}{10}\left[\frac{3}{2}\exp(-((R_s^{(1)} + R_c^{(1)})/2 - i\omega_Q/2)t_1) + \exp(-R_c^{(1)}t_1) + \frac{3}{2}\exp(-((R_s^{(1)} + R_c^{(1)})/2 + i\omega_Q/2)t_1)\right]\exp(-R_c^{(1)}t_2) \\ & + \frac{3}{20}\left[\frac{3}{2}\exp(-R_s^{(1)}t_1) + \exp(-((R_s^{(1)} + R_c^{(1)})/2 + i\omega_Q/2)t_1) - \frac{1}{2}\exp(-(R_s^{(1)} + i\omega_Q)t_1)\right]\exp(-(R_s^{(1)} + i\omega_Q)t_2) \end{aligned}$$

(QE experiment) [70]

where we have used the simplified expressions in Eq. [47], valid for $\omega_Q \gg J_2$. A simulated 2D contour spectrum is shown in Fig. 5. A slice along F_1 at the satellite position in F_2 shows peaks at frequencies 0, $\pm\omega_Q/2$, and $\pm\omega_Q$, with the positive and negative frequencies pertaining to the two satellites in F_2 (Fig. 6). The peaks at zero frequency in F_1 are free from broadening because of a possible inhomogeneity in

splitting and are designated for the measurement of the satellite relaxation rate $R_s^{(1)}$. However, for small splitting or if the satellites are spread out over a large frequency range, overlap of the various signal contributions is unavoidable. This makes an accurate measurement of the natural line widths difficult, if not impossible. If the signals can not be separated to a sufficient extent, slow dynamics is probed more efficiently by applying a lock through an RF field as will be reviewed in part II (*6, 18*).

In the case of the DQ-MA and JB experiments, a similar strategy can be applied, with the exception that here no central signal contribution is observed. As an example, we give the result for the DQ-MA experiment with delayed acquisition after the formation of the primary echo

$$\pi/2(\phi) - \text{evolution}, t_1/2 - 54.7°(\phi) - \text{mixing}, t_m - 54.7°(0) - \text{evolution}, t_1/2 - \text{acquire}, t_2 \quad [71]$$

where the phase ϕ is stepped through 0, 90, 180, and 270°, while the receiver phase is alternated. If we neglect the time evolution during the mixing period (a few microseconds), the signal can be calculated easily:

$$s(t_1, t_2, p = 2) = 2/3 f_{21}^{(1)}(t_1/2) f_{12}^{(1)}(t_1/2 + t_2) \quad [72]$$

Again, to identify the various signal contributions, the evolution functions are expanded ($\omega_Q \gg J_2$)

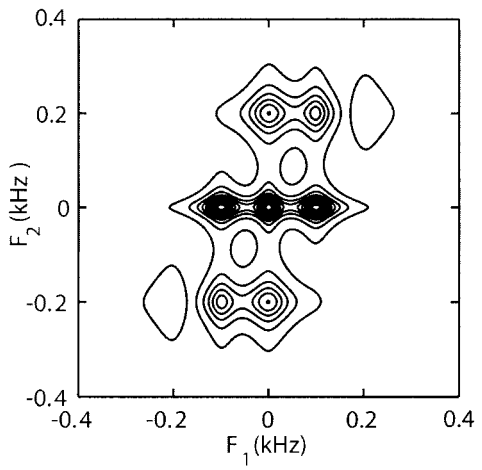

Figure 5 Simulated spectrum (contour plot) pertaining to the QE experiment with the same parameters as in Fig. 4. Notice that the phase information is lost because the absolute value of the spectrum is displayed.

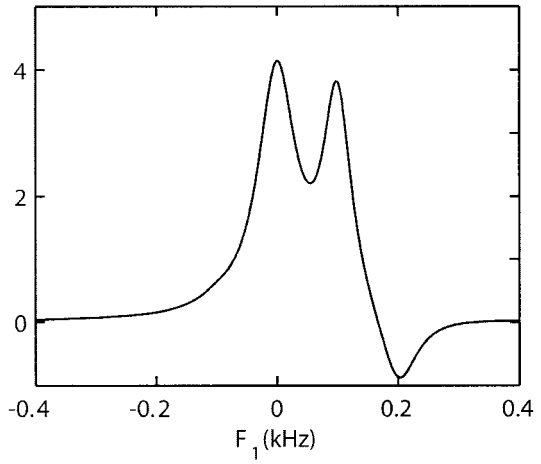

Figure 6 Slice along F_1 at the satellite position in F_2 of the simulated QE spectrum shown in Fig. 5. Notice that the peak at $F_1 = 0$ is free from broadening related to a possible inhomogeneous quadrupolar splitting and has a width given by the satellite relaxation rate $R_s^{(1)}$.

$$s(t_1, t_2) = \frac{1}{10}([\exp(-(R_s^{(1)} - i\omega_Q)t_1) - \exp(-R_s^{(1)}t_1)]\exp(-(R_s^{(1)} - i\omega_Q)t_2) - [\exp(-R_s^{(1)}t_1) - \exp(-(R_s^{(1)} + i\omega_Q)t_1)] \times \exp(-(R_s^{(1)} + i\omega_Q)t_2)) \quad \text{(DQ-MA experiment)} \quad [73]$$

In the 2D spectrum, a slice along F_1 at the satellite positions in F_2 shows peaks at frequencies 0 and $\pm\omega_Q$ (with the positive and negative frequencies pertaining to the two different satellites in F_2). As in the case of the QE experiment, the peaks at zero frequency in F_1 are free from inhomogeneous broadening and are designated for measurement of the satellite relaxation rate $R_s^{(1)}$. For the JB experiment with delayed acquisition, a similar expression can be derived.

CONCLUSIONS

The irreducible tensor operator formalism is particularly suitable to follow the destiny of the spin-3/2 density operator under a series of RF pulses and evolution intervals in the presence of fluctuating and static quadrupolar interactions. The NMR line shapes are analyzed for any value of the static quadrupolar interaction, ranging from isotropic systems to systems exhibiting large splitting far exceeding the line widths. Multiple-quantum filtration techniques allow

the selective detection of nuclei involved in slow molecular motion and/or in an ordered, liquid crystalline environment. The latter phenomenon relies on the unique formation of rank-two coherence order in the presence of a static quadrupolar coupling. Slow molecular motion is probed through transverse relaxation via the spectral density at zero frequency, but the relevant line widths may be broadened by an inhomogeneity in static quadrupolar coupling. To a certain extent, this effect can be eliminated by delayed acquisition schemes. However, for small splitting or if the satellite signals are spread out over a large frequency range, overlap of the satellite signal contributions is unavoidable. If the satellite signals can not be separated to a sufficient degree, slow dynamics is probed more efficiently by applying a lock through an RF field. The dynamics of spin 3/2 under spin-locking conditions will be reviewed in part II.

REFERENCES

1. Meersmann T, Smith SA, Bodenhausen G. 1998. Multiple-quantum filtered Xenon-131 NMR as a surface probe. Phys Rev Lett 80:1398–1401.
2. Delville A, Porion P, Faugere AM. 2000. Ion diffusion within charged porous network as probed by nuclear quadrupolar relaxation. J Phys Chem B 104:1546–1551.
3. Groot LCA, van der Maarel JRC, Leyte JC. 1994. ^{23}Na-relaxation in isotropic and anisotropic liquid-crystalline DNA solutions. J Phys Chem 98:2699–2705.
4. Stein VM, Bond JP, Capp MW, Anderson CF, Record MT. 1995. Importance of coulombic end effects on cation accumulation near oligoelectrolyte B-DNA—a demonstration using Na-23 NMR. Biophys J 68:1063–1072.
5. Porion P, Al Muhktar M, Meyer S, Faugère AM, van der Maarel JRC, Delville A. 2001. Nematic ordering of suspensions of charged anisotropic colloids detected by ^{23}Na nuclear magnetic resonance. J Phys Chem B 105: 10505–10514.
6. van der Maarel JRC, Woessner DE, Merritt ME. 2002. Extremely slow counterion dynamics in Xanthan liquid crystal through ^{23}Na and ^{14}N NMR. J Phys Chem B 106:3864–3871.
7. Eliav U, Navon G. 1994. Analysis of double-quantum filtered NMR spectra of Na-23 in biological tissues. J Magn Reson B 103:19–29.
8. Hilal S, Oh C, Mun I, Silver A. 1992. Sodium imaging. In: Stark D, Bradley W, editors. Magnetic Resonance Imaging. St. Louis, MO: Mosby.
9. Chen SWW, Rossky PJ. 1993. Influence of solvent and counterion on Na-23 spin relaxation in aqueous solution. J Phys Chem 97:10803–10812.
10. Abragam A. 1961. Principles of nuclear magnetism. Oxford: Clarendon.
11. Bowden GJ, Hutchison WD. 1986. Tensor operator formalism for multiple-quantum NMR. 1. Spin-1 nuclei. J Magn Reson 67:403–414.
12. Bowden GJ, Hutchison WD, Khachan J. 1986. Tensor operator formalism for multiple-quantum NMR. 2. Spins 3/2, 2, and 5/2 and general I. J Magn Reson 67:415–437.
13. Rose ME. 1957. Elementary theory of angular momentum. New York: Wiley.
14. Woessner DE. 2001. NMR relaxation of spin-3/2 nuclei: Effects of structure, order, and dynamics in aqueous heterogeneous systems. Concepts Magn Reson 13: 294–325.
15. Wokaun A, Ernst RR. 1977. Selective excitation and detection in multilevel spin systems: Application of single transition operators. J Chem Phys 67:1752–1758.
16. Pandey L, Towta S, Hughes DG. 1986. NMR pulse response and measurement of the quadrupolar coupling constant of $I = 3/2$ nuclei. J Chem Phys 85:6923–6927.
17. Hancu I, van der Maarel JRC, Boada FE. 2000. A model for the dynamics of spins 3/2 in biological media: Signal loss during radio frequency excitation in triple-quantum-filtered sodium MRI. J Magn Reson 147:179–191.
18. van der Maarel JRC, Jesse W, Hancu I, Woessner DE. 2001. Dynamics of spin $I = 3/2$ under spin-locking conditions in an ordered environment. J Magn Reson 151:298–313.
19. Campolieti G, Sanctuary BC, Cole HBR. 1990. Multipole theory of soft pulses in NMR of quadrupolar solids. J Magn Reson 88:457–472.
20. Jaccard G, Wimperis S, Bodenhausen G. 1986. Multiple-quantum NMR spectroscopy of $S = 3/2$ spins in isotropic phase: A new probe for multiexponential relaxation. J Chem Phys 85:6282–6293.
21. Lurçat F. 1956. Saturation et relaxation en résonance nucléaire (magnétique et quadrupolaire). Temps et modes de relaxation en relaxation paramagnétique. Arch Sci 9:166–169.
22. Lurçat F. 1955. Sur la relation entre les temps de relaxation et les probalités de transition en resonance nucléaire (magnétique et quadrupolaire). I. Comptes Rendus 240:2402–2403, 2517–2518.
23. McLachlan AD. 1964. Line widths of electron resonance spectra in solution. Proc R Soc Lond A280:271–288.
24. Hubbard PS. 1970. Nonexponential nuclear magnetic relaxation by quadrupolar interactions. J Chem Phys 53:985–987.
25. Pekar J, Leigh Jr JS. 1986. Detection of biexponential relaxation in sodium-23 facilitated by double-quantum filtering. J Magn Reson 69:582–584.
26. Werbelow L, Pouzard G. 1981. Quadrupolar relaxation. The multiquantum coherences. J Phys Chem 85:3887–3891.
27. Werbelow LG, Marshall AG. 1981. The NMR of spin-

3/2 nuclei: The effect of second-order dynamic frequency shifts. J Magn Reson 43:443–448.
28. Tromp RH, de Bleijser J, Leyte JC. 1990. Nuclear magnetic dynamic shift in an isotropic system. Chem Phys Lett 175:568–574.
29. Eliav U, Shinar H, Navon G. 1991. An observation of ^{23}Na NMR triple-quantum dynamic shift in solution. J Magn Reson 94:439–444.
30. Dinesen TRJ, Sanctuary BC. 1994. Relaxation of anisotropically oriented $I = 3/2$ nuclei in the multipole basis: Evolution of the second rank tensor in the double quantum filtered nuclear magnetic resonance experiment. J Chem Phys 101:7372–7380.
31. van der Maarel JRC. 1989. Relaxation of Spin $S = 3/2$ in a nonzero average electric field gradient. Chem Phys Lett 155:288–296.
32. Einarsson L, Westlund PO. 1988. The effects of higher rank multipoles on relaxation measurements in isotropic high spin systems. J Magn Reson 79:54–65.
33. Chung CW, Wimperis S. 1990. Optimum detection of spin-3/2 biexponential relaxation using multiple-quantum filtration techniques. J Magn Reson 88:440–447.
34. Kemp-Harper R, Brown SP, Hughes CE, Styles P, Wimperis S. 1997. Na-23 NMR methods for selective observation of sodium ions in ordered environments. Prog Nucl Magn Reson Spectrosc 30:157–181.
35. Navon G, Shinar H, Eliav U, Seo Y. 2001. Multiquantum filters and order in tissues. NMR Biomed 14:112–132.
36. Hancu I, van der Maarel JRC, Boada FE. 2002. Detection of sodium ions in anisotropic environments through spin-lock NMR. Magn Reson Med 47:68–74.
37. Ernst RR, Bodenhausen G, Wokaun A. 1987. Principles of nuclear magnetic resonance in one and two dimensions. Oxford: Clarendon p 338–340.
38. Furo I, Halle B, Wong TC. 1988. Spin relaxation of $I > 1$ nuclei in anisotropic systems. I. Two-dimensional quadrupolar echo Fourier spectroscopy. J Chem Phys 89:5382–5397.
39. Furo I, Halle B. 1992. 2D Quadrupolar-echo spectroscopy with coherence selection and optimized pulse angle. J Magn Reson 98:388–407.

BIOGRAPHY

Johan van der Maarel was born in 1960 in Maassluis, The Netherlands. He received his Ph.D. in physical chemistry from Leiden University in 1987. His doctoral work was on the structure and dynamics of water and aqueous solutions. Since then, he has been employed as a Lecturer in Physical and Macromolecular Chemistry and has spent a sabbatical as visiting professor at the University of Minnesota, U.S.A. His research is concerned with the NMR technique, but he also applies scattering methods to complex fluid systems. He has been performing studies of polyelectrolytes, polyelectrolyte diblock copolymer micelles, and mesostructures of DNA.